Geophysical Research Letters

RESEARCH LETTER
10.1029/2018GL080384

Contrasting Mechanical and Hydraulic Properties of Wet and Dry Fault Zones in a Proposed Shale-Hosted Nuclear Waste Repository

Luis Felipe Orellana[1,2], **Carolina Giorgetti**[1], **and Marie Violay**[1]

[1]Laboratory of Experimental Rock Mechanics, IIC-ENAC, École Polytechnique Fédérale de Lausanne, Lausanne, Switzerland, [2]Now at Laboratory of Rock Mechanics, DIMIN, FCFM, Universidad de Chile, Santiago, Chile

Key Points:
- Dry samples are weak and shift from unstable to stable fault slip behavior when increasing sliding velocity
- Wet samples exhibit velocity-strengthening behavior, and water reduces the coefficient of friction to ~45% of dry samples
- Shear deformation is accompanied by shear dilatancy and enhanced permeability

Supporting Information:
- Supporting Information S1

Correspondence to:
L. F. Orellana,
luisfelipe.orellana@ing.uchile.cl

Citation:
Orellana, L. F., Giorgetti, C., & Violay, M. (2019). Contrasting mechanical and hydraulic properties of wet and dry fault zones in a proposed shale-hosted nuclear waste repository. *Geophysical Research Letters*, *46*, 1357–1366. https://doi.org/10.1029/2018GL080384

Received 10 SEP 2018
Accepted 24 JAN 2019
Accepted article online 29 JAN 2019
Published online 14 FEB 2019

Abstract The underground disposal of high-level nuclear waste is a pressing issue for several countries. In Switzerland, the Opalinus Clay formation is a shale with favorable barrier properties. However, small-to-large faults intersecting the formation bring the long-term integrity of the future repositories into question. Here we present the first systematic laboratory study on the frictional strength, stability, dilatancy, and permeability of simulated Opalinus Clay gouge under typical repository conditions. Wet gouges exhibit an extremely low coefficient of friction (μ_f~0.16), velocity-strengthening behavior, and shear-enhanced dilatancy at the onset of slip, and permeability increase. Conversely, dry gouges remain weak (μ_f~0.36) but exhibit a transition from unstable to stable sliding with increasing sliding velocity. Thus, we infer that faults hosted in Opalinus Clay could be easily reactivated via aseismic creep, possibly acting as poor fluid conduits. However, if temporarily dried, the faults become potentially unstable, at least, at low sliding velocities (<~10 μm/s).

Plain Language Summary In Switzerland, the Opalinus Clay formation is a shale under study as a host-rock for deep underground nuclear waste storage. The Opalinus Clay formation has favorable barrier properties, yet small-to-large faults intersecting the formations bring the long-term integrity of the future repositories into question. In particular, induced seismicity and the creation of preferential fluid paths are of concern. Here we present the first systematic laboratory study addressing those issues. Experiments show that under representative conditions for deep nuclear waste storage, faults exhibit extremely low frictional strength and they show stable fault slip behavior. Moreover, at the onset of slip, dilatancy and permeability increase are observed. Hence, we infer that faults hosted in Opalinus Clay formation could be easily reactivated without generating earthquakes, but possibly acting as weak fluid conduits. However, if faults temporarily dried, they could become potentially unstable, a scenario that anyway will not produce large earthquakes.

1. Introduction

Deep geological repositories (DGR) are the most promising solution for the long-term confinement and isolation of high-level nuclear waste (Tsang et al., 2015). In Switzerland, the concept for DGR is developed at the Mont Terri Laboratory (MTL), an underground research facility that runs site characterization and testing activities in the Opalinus Clay (OPA) formation (Nussbaum et al., 2011). The OPA formation corresponds to an indurated, hydromechanically anisotropic shale that has favorable transport (e.g., low permeability) and geochemical barrier properties for the retention of radionuclides (Bossart et al., 2017).

At the MTL, small-to-large tectonic fault systems intersect the OPA formation. For instance, the "Main Fault" (MF), a 1.0- to 4.2-m-thick thrust fault, crosscuts the MTL at a depth of ~300 m (Figure 1a). Within the limits of the MF, various structural elements are recognizable such as fractures, secondary shear planes, scaly clays, and fault gouge (Nussbaum et al., 2011). While there will not be any disposal of radioactive waste at the MTL, the presence of faults within the OPA formation poses questions about the final site regions. Indeed, faults have the potential to damage the underground infrastructure (e.g., via sudden fault slip events) and to allow the migration of stored radionuclides (e.g., as permeable drainage paths; Tsang et al., 2015; Wang et al., 2001; Figure 1b).

Recent in situ fluid-injection experiments at the MTL activated the MF, resulting in limited displacement accompanied by a sequence of seismic events within the fault zone (Guglielmi et al., 2017; Jeanne et al.,

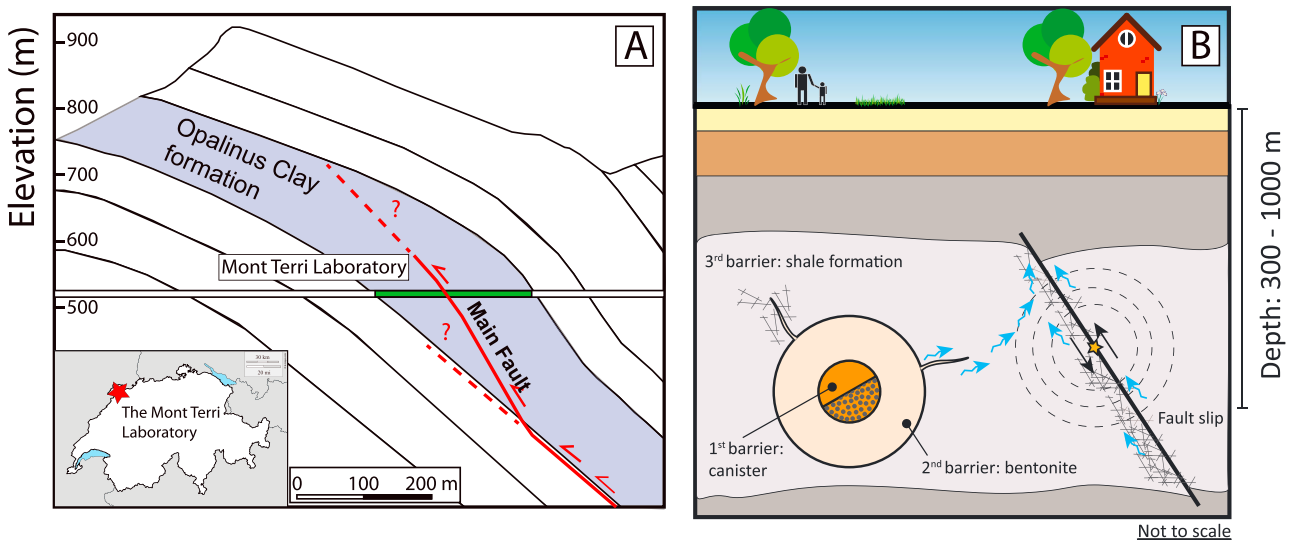

Figure 1. (a) Cross section of the OPA formation showing the location of the MTL and the MF crosscutting the laboratory. Inlet shows the site of the MTL in the northern part of Switzerland. (b) A schematic representation of DGR risks (modified from Rutqvist et al. (2014)) including potential seismicity and creation of permeable drainage paths.

2017, 2018). Moreover, permeability measurements coupled with fault displacement in the same experiments revealed a permeability increase associated with shear-enhanced dilatancy.

Furthermore, during the operation of the DGR, heating generated from high-level nuclear waste can affect the host-rock and adjacent fault systems. Indeed, temperature can exceed 50–70 °C for long periods of times (~10,000 years) in the surroundings (~10 m) of the heating source (Heierli & Genoni, 2017; Yang & Yeh, 2009), leading to temperature gradients and dehydration processes (Buscheck et al., 2002), which will tend to dry the rock, create pore overpressures, and change the natural permeability of the host-rock (Tsang et al., 2012).

Despite recent efforts, how the evolution of fault slip on preexisting faults in the OPA formation (seismic or aseismic) and how fault permeability changes during shear deformation (enhancement or destruction) still are not well understood, yet they are crucial to the long-term integrity of the repositories. Thus, further investigations of the frictional properties, shear-enhanced dilatancy, and the couplings governing slip stability in OPA fault arrays are still needed.

Frictional properties of OPA have been recently studied (Fang et al., 2017, 2018; Orellana et al., 2018b) in the context of rate-and-state theory (Dieterich, 1978; Ruina, 1983). However, these laboratory studies were run in partially saturated conditions or with limited normal stress range. Nevertheless, they have shown a significant frictional weakness relative to framework silicates and carbonates (Byerlee, 1978) and, at slip velocities (<1 mm/s), velocity-strengthening behavior, that is, aseismic, similar to other clay-rich rocks (e.g., Behnsen & Faulkner, 2012; Ikari et al., 2009; Saffer & Marone, 2003).

Laboratory tests have shown that once fault slip on preexisting faults in shales occurs, fault permeability can be either depleted or enhanced. Permeability might decrease thank to shear-enhanced compaction (Crawford et al., 2008), swelling of clays (Cuss et al., 2011; Fang et al., 2017, 2018), and clay-fabric development (Ikari et al., 2009). Conversely, permeability might increase due to deformation-induced dilatancy when sheared at low to moderate effective stresses (Im et al., 2018; Lefèvre et al., 2016; Wu et al., 2017; Zhang & Cox, 2000).

The strategy of this study includes frictional sliding experiments in a triaxial saw-cut configuration at different effective normal stresses which are representative of future in situ conditions. We have run tests at sliding velocities and saturation conditions (dry and wet) that have not been previously tested. Dry and wet conditions represent end-member environments of the operation of DGR. Further, we examine dilatancy and compaction behavior via volumetric pore fluid changes in the gouge layer, and we measure

permeability before and after shearing. Here we attempt to quantify the frictional strength, stability, dilatancy, and permeability variations of the OPA formation and its implications for the DGR concept in clay-rich formations.

2. Methods

We have used simulated fault gouge samples that were prepared from nondeformed OPA. Samples were crushed and then sieved to ensure average and maximum grain sizes of 7.0 and 125 μm, respectively. The mineral composition of the simulated OPA fault gouge consists of phyllosilicates (~51%), quartz (~23%), and calcite (~14%). Among the phyllosilicates, kaolinite, mica, and chlorite are the main components comprising ~28%, ~10%, and ~9% of the total weight content, respectively (Table 1a in the supporting information). Both composition and grain sizes are representative of natural fault gouge (Orellana et al., 2018b).

We performed frictional tests using a triaxial deformation apparatus with a servo-controlled axial system, and fluid pressure pumps. The tests were conducted on an ~1.0-mm-thick gouge layer using a saw-cut configuration. The experimental assembly consists of two cylindrical stainless-steel pistons of 38 mm in diameter cut along a plane inclined 30° to the cylindrical axis with a surface roughness of 12.5 μm. At each end of the piston assembly, a high-permeability (10^{-12} m^2) sintered porous stainless-steel filter of 3.8 mm in diameter was placed to allow fluid flow through the sample (Figure 2a).

Samples were first dried for 48 hr at 50°. In this way, while some small fraction of water could still be present, in this study 1), we replicate dry conditions similar to those expected during the operation of the nuclear waste repository (Heierli & Genoni, 2017; Yang & Yeh, 2009) and 2) we have ensured that any thermal damage to the mineral grains was avoided (Rutter & Mecklenburgh, 2018). For wet experiments, 5 g of dried powdered OPA was mixed with ~2.5 mL of deionized water to make a paste (Lockner et al., 2011; Tembe et al., 2010). The sample was then spread onto the saw-cut surface of the lower piston and sandwiched by the upper stainless-steel piston. The assembly could sit for at least 48 hr, as pore volumes and pressures equilibrated to ensure fully saturated conditions.

We ran the experiments at room temperature, and at different constant effective normal stress ranging from 4 to 20 MPa. Pore pressure, if present, was fixed to 10 MPa. Each experiment followed a common displacement history (Figure 2b). The initial axial loading rate for the first 2.0 mm was 1 μm/s, that is, a sliding velocity of 1.14 μm/s and a strain rate of $\gamma \approx 0.001$ s^{-1} along the fault. After 2.0 mm of axial displacement, the samples were subjected to a sequence of increasing axial velocity steps: 0.01–0.1, 0.1–1, and 1–10 μm/s for 0.2 mm each. These rates were slow enough to ensure controlled pore fluid pressures (Faulkner et al., 2018; Morrow et al., 2017). However, localization within clay-rich shear planes during deformation and the inherent low permeability of the material can generate very local fluid overpressures and nondrained conditions in the surroundings of the shear planes that are impossible to control.

Friction (μ) was calculated as

$$\mu = \frac{\tau}{\sigma_n'} = \frac{\tau}{\sigma_n - Pp} \tag{1}$$

where τ corresponds to the shear strength parallel to the fault, σ_n is the normal stress, Pp is the pore pressure, and σ_n' is the effective normal stress. Shear strength (τ) was corrected for the decreasing contact area with slip. Friction (μ) values were obtained at 2 mm of axial displacement, before velocity steps started (Figure 2b). At low σ_n, friction is overestimated if the inherent shear strength or equivalent cohesion (S_o) is not considered (Jaeger et al., 2007). Thus, we have calculated the coefficient of friction (μ_f) and S_o as the best fit to the tangent of the $\tau - \sigma_n'$ curve as

$$\mu_f = \frac{\tau - S_o}{\sigma_n'} = \frac{\tau - S_o}{\sigma_n - Pp} \tag{2}$$

The values of μ and μ_f are related as

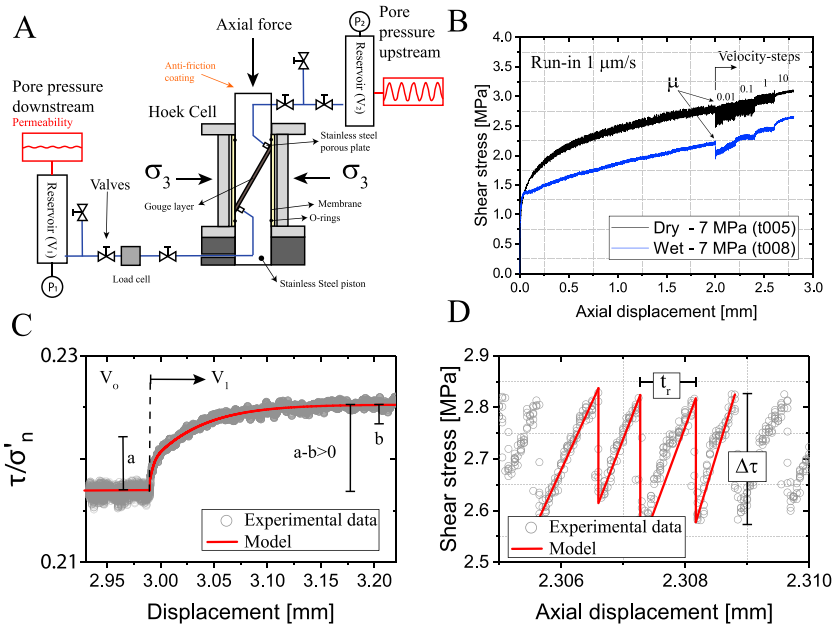

Figure 2. Experimental setup, frictional tests, and quantification of frictional properties. (a) Saw-cut and pore pressure pump configuration. (b) Typical shear curves for wet and dry tests. Run-in velocity is of 1 μm/s. (c) Model inversion of the experimental data with slip law resulting in rate-and-state values of a and b. (d) Stress drop and recurrence time of the stick–slip events.

$$\mu = \frac{\tau}{\sigma_n{}'} = \frac{\tau}{\sigma_n - Pp} = \frac{S_o}{\sigma_n - Pp} + \mu_f \tag{3}$$

To understand fault stability, we modeled each velocity step using the empirical Ruina's slip-dependent evolution law (Ruina, 1983), through a least squares numerical fitting routine (Noda & Shimamoto, 2009). The frictional rate parameters a and b describe the dependence of friction on sliding velocity as

$$a - b = \frac{\Delta\mu_{ss}}{\ln\left(\frac{V}{V_o}\right)} \tag{4}$$

where $\Delta\mu_{ss}$ is the change in the steady state friction upon an immediate change in sliding velocity from V_o to V (Scholz, 2002). When $(a - b) \geq 0$ fault slip occurs in a stable manner, that is, velocity-strengthening behavior. If $(a - b) < 0$ fault slip will potentially develop in an unstable fashion, that is, velocity-weakening behavior (Jaeger et al., 2007; Figure 2c). When necessary, we removed the long-term strain hardening reflected in linear strengthening, assuming that the strengthening is independent of the velocity dependence of friction (Samuelson et al., 2009). When stick–slip behavior occurs, magnitudes of $(a - b)$ cannot be directly computed. Thus, we have inferred velocity-weakening and calculated average stress drops ($\Delta\tau$; Figure 2d).

We carried out fault-parallel permeability measurements before ($k_{i,\ //}$) and after ($k_{f,\ //}$) shearing using the pore pressure oscillation method (Bernabé et al., 2006; Faulkner & Rutter, 2000). We also monitored the evolution of pore volumes while keeping Pp constant to evaluate potential shear-enhanced compaction or dilatancy of the samples (Behnsen & Faulkner, 2012; French et al., 2015). For more details on the experimental methods, please refer to the supporting information.

3. Results

At 1.14-μm/s sliding velocity, our results show μ values ranging from 0.18 to 0.32 for wet samples, and 0.33 to 0.45 for dry samples (Figure 3a). Wet and dry friction decreases with increasing σ'_n (Figure 3a). Cohesion is

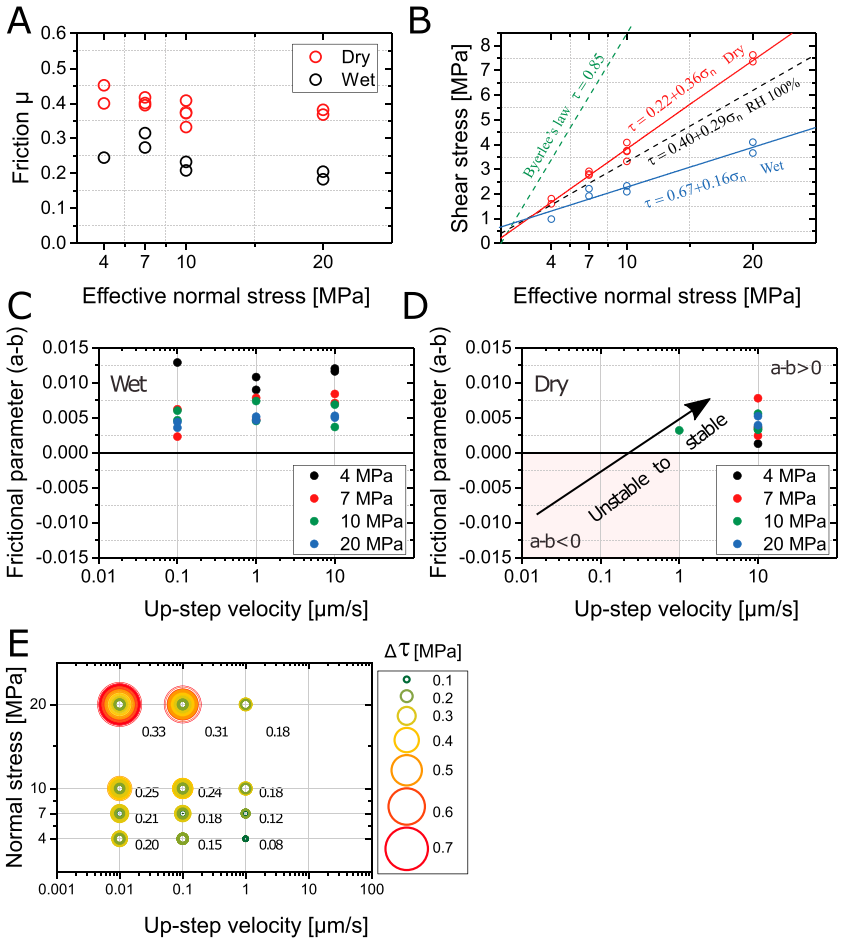

Figure 3. Frictional results. (a) Friction at 2-mm axial displacement and (b) shear stress versus effective normal stress for wet and dry samples. For comparison, we have included the Byerlee's law and previous results of frictional experiments carried out at 100% room humidity condition (Orellana et al., 2018b). Frictional parameter versus axial velocity for (c) wet and (d) dry samples. (e) Stress drops for selected experiments (t015, t005, t018, t023).

then estimated, giving $\mu_f = 0.16$ and $S_o = 0.67$ MPa for wet samples, and $\mu_f = 0.36$ and $S_o = 0.22$ for dry samples (Figure 3b).

Regarding fault stability, wet experiments show a consistent velocity-strengthening behavior with values of $(a - b)$ between 0.002 and 0.013 at all up-step velocities (Figure 3c). Dry experiments undergo a transition from unstable behavior, that is, stick–slip, to stable behavior above slip rates of 10 μm/s, with $(a - b)$ values between 0.001 and 0.008 (Figure 3d). When stick–slip occur, we record more than 50 events, with recurrence times up to 145 s and average $\Delta\tau$ ranging from 0.05 to 0.56 MPa (Figure 3e). At low σ_n and slow sliding velocities, stick–slip events have systematically smaller $\Delta\tau$ and are less regular than their higher σ_n counterparts. For example, at the same axial velocity of 0.01 μm/s, the average $\Delta\tau$ is 0.20 at $\sigma'_n = 4$ MPa, while 0.33 at 20 MPa. Finally, $\Delta\tau$ amplitudes decrease when increasing velocity for all tests.

In our tests, permeability increases from $k_{i,//} = 2.02 \times 10^{-20}$ to $k_{f,//} = 2.71 \times 10^{-20}$ when samples are sheared at $\sigma'_n = 4$ MPa, and from 6.15×10^{-21} to 1.78×10^{-20} when $\sigma'_n = 20$ MPa (Figure 4a). These measurements indicate that after shearing, permeability increases by a factor of ~3 and reaches values of ~10^{-20} m^2. The pore volume evolution during shearing suggests dilatancy during the first ~1.0–1.5 mm of axial displacement followed by a slight compaction and/or a steady state porosity until 2 mm of axial displacement is reached (Figure 4b). Once the velocity step sequence starts, dilatancy or compaction occurs depending on the velocity history and σ'_n.

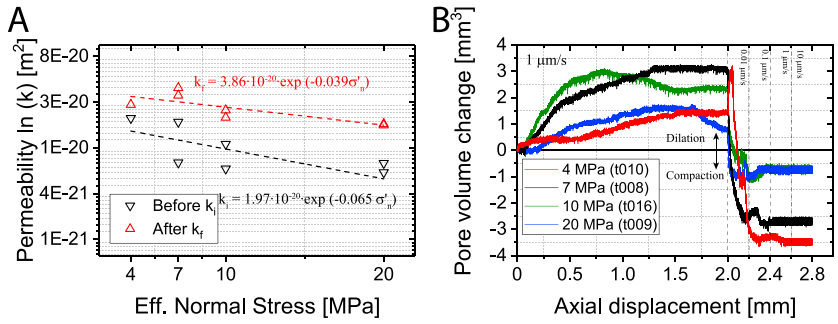

Figure 4. (a) Permeability measurements parallel to the direction of shearing before and after the shearing stage. (b) The change in pore volume during shearing for selected samples (t010, t008, t016, t009). Compaction corresponds to negative pore volume change.

4. Discussion

4.1. Frictional Strength

Clays exert a remarkably strong control in reducing the frictional strength of fault rocks in particular when the clay content is higher than ~15–30% (Logan & Rauenzahn, 1987; Morrow et al., 2017; Saffer & Marone, 2003). The presence of large amounts of clays in our samples (~50%) is sufficient to explain the overall strength reduction of the simulated fault gouge with respect to the Byerlee's law ($\mu \approx 0.85$; Byerlee, 1978), and is also consistent with previous studies on clay-rich materials ($\mu_f \approx 0.2 - 0.6$; e.g., Behnsen & Faulkner, 2012; Ikari et al., 2007, 2009; Kohli & Zoback, 2013; Morrow et al., 2000; Saffer & Marone, 2003; Scuderi & Collettini, 2018).

The frictional strength (μ_f) of OPA (equations (2) and (3) and Figure 3a) appears strongly dependent on whether the sample is dry or wet for the full range of σ'_n tested (Ikari et al., 2007; Morrow et al., 2017). We show that dry samples are weak ($\mu_f \approx 0.36$) and are weaker ($\mu_f \approx 0.16$) when wet. The strong weakening enhanced by the presence of water may be, in addition to realignment of clay minerals and shear localization (Logan & Chester, 1987; Numelin et al., 2007; Saffer et al., 2001), to the lubrication effect of water films within the clay-rich shear planes, as inferred by previous studies (e.g., Ikari et al., 2007; Moore & Lockner, 2004, 2007; Morrow et al., 2000).

Previous frictional experiments performed on OPA gouge at 100% relative humidity, that is, partially saturated condition (Orellana et al., 2018b), exhibited μ_f values between the results of this study (Figure 3b), which were higher than our values of wet friction, that is, $\mu_{f,\,wet} < \mu_{f,\,RH100\%} < \mu_{f,\,dry}$. Taken together, our results highlight the strong effect of water on the frictional weakness of faults hosting OPA, suggesting that small pore fluid or stress field perturbations could result in their activation.

4.2. Frictional Stability

Previous work on OPA gouge samples has shown velocity-strengthening behavior (Fang et al., 2017, 2018; Orellana et al., 2018b). Our wet sample data are consistent with those studies, and also with others on clay-rich samples (e.g., Ikari et al., 2009; Morrow et al., 2017; Tembe et al., 2010). Interestingly, within the same range of low σ'_n, our dry gouges exhibit stick slips behavior (inferred to be a manifestation of velocity-weakening friction) at slow velocities (<10 μm/s) and shift to velocity-strengthening when increasing sliding velocity (≥10 μm/s). Few examples in the literature indicate that clay-rich materials are velocity-weakening at slow velocities (≤20 μm/s). Unstable slip behavior has been observed (1) when clay content is less than 30% (Kohli & Zoback, 2013), (2) under dry conditions and low σ'_n in smectite (Ferri et al., 2011; Saffer et al., 2001; Saffer & Marone, 2003) and montmorillonite-bearing samples (Ikari et al., 2007; Logan & Rauenzahn, 1987), and (3) due to preexisting clay-fabric (Orellana et al., 2018a).

In our tests, velocity-strengthening behavior dominates in wet samples. Stick–slip events are observed only in dry gouges at slow sliding velocities. Then, the transition between unstable and stable frictional behavior can be explained in terms of deformation and frictional healing processes that occur depending upon the absence or presence of pore fluids.

First, in clays, the reorientation and preferential alignment of clay minerals along shear planes with shearing result in shear localization and foliation development (Logan & Chester, 1987; Numelin et al., 2007). Under dry conditions, cataclastic deformation mechanisms, including frictional sliding at grain contacts, distributed and chaotic granular flow, and grain fracturing, are dominant processes (Moore & Lockner, 2007). Thus, the dry samples possibly deform in a distributed manner, resulting in relatively higher friction (Figures 3a and 3b). Conversely, the presence of pore fluids in clays facilitates a lubricating effect between grains promoting shear localization of strain along well-defined clay-rich planes (Morrow et al., 2000; Shimamoto & Logan, 1981; Tembe et al., 2010) resulting in lower friction and velocity-strengthening behavior as observed in our wet gouges (Figures 3a–3c). Unfortunately, we were not able to analyze microstructures to test this hypothesis.

Then, in dry samples, frictional healing processes can partially explain the transition from unstable to stable sliding that occurs at velocities smaller than a reference cutoff velocity v_* (i.e., $v < v_* \approx 10$ μm/s). We infer that these stick slips would be expected due to the potential aging of contacts, that is, fault restrengthening, associated with frictional healing processes with slip, such as ploughing, shear-enhanced indentation, shear-enhanced compaction, or a combination of the above (Marone & Saffer, 2015). When $v > v_*$, frictional healing is possibly negligible because it is not effective at high sliding velocities, as the time needed for appreciable healing is longer than the time over which contacts are continuously renewed at higher sliding velocities (Bar-sinai et al., 2014; Kuwano et al., 2013). This observation is also supported by frictional healing rates (β) previously measured in the same OPA gouge samples during slide-hold-slide tests (Orellana et al., 2018b). This study shows higher values of β for dry samples than for partially saturated samples, that is, $\beta_{100RH} < \beta_{dry}$. In our wet samples, we expect even smaller values of β, that is, $\beta_{wet} < \beta_{100\ \%\ RH} < \beta_{dry}$, and therefore null frictional re-strengthening over time, in agreement with the velocity-strengthening behavior observed in our tests (Figure 3c). Furthermore, our results show that the magnitude of the $\Delta\tau$ increases with increasing σ_n (Figure 3e). This effect is a consequence of the interplay between the increase in fault stiffness with σ_n and the constant machine stiffness, as the rate-and-state friction theory predicts (Baumberger & Berthoud, 1999; Leeman et al., 2016; see supporting information).

The stick–slip behavior shown by dry samples, though characterized by small stress drops ($\Delta\tau \leq 0.35$ MPa, $\Delta\tau/\tau \leq 5\%$), are manifestations of fault instability (Brace & Byerlee, 1966). However, the conditions for instability do not persist as slip velocity increases, as indicated by the transition to velocity-strengthening when increasing velocity.

Finally, and based on these observations, we infer that faults within the OPA formation under water-saturated conditions will tend to slip stably via aseismic creep. Nonetheless, our results illustrate the key role played by water in stabilizing fault slip, at least at slow velocities.

4.3. Permeability Evolution and Shear-Enhanced Dilation

Values of $k_{i,\,//}$ and $k_{f,\,//}$ ($10^{-21} - 10^{-20}$) are in the same range as values previously reported for nondeformed rock (Senger et al., 2018; Yu et al., 2017). Our data suggest a shear-enhanced fault-parallel permeability at slow sliding velocities (<1 μm/s) and at low σ'_n in agreement with previous tests on clay-rich samples (Wu et al., 2017; Zhang & Cox, 2000). This increase suggests that the during slip events a fault within the OPA formation could act as a poor conduit with respect to the surrounding nondeformed rock.

Consistent with the permeability increase upon shear deformation, the evolution of pore volumes during shearing suggests a predominant shear-enhanced dilatancy, at least for the first 2 mm of displacement (Figure 4b). When the sliding velocity suddenly decreases to 0.01 μm/s at the beginning of the velocity-step sequence, shear-enhanced compaction occurs under quasi-stationary contact for ~5.5 hr, indicating a rearrangement of the pore structure. The velocity- and stress-dependent dilation or compaction observed during the velocity sequences implies a competition between continuous creation and destruction of dilatant regions within the gouge sample related to its velocity history, which in turn will create and destroy fluid-flow pathways that affect permeability. In our tests, the initial dilatancy during the first 2 mm of displacement along with the measured permeability increase after shearing suggests that the shear deformation of the gouge results in the development of poor fluid pathways. More experiments are needed to understand the micromechanisms governing this competition fully.

5. Conclusions and Implications for Nuclear Waste Repositories

While it is most likely that DGR will be placed far from fault systems, the identification of these faults remains challenging in shale formations. Therefore, risks associated to fault reactivation and induced seismicity cannot be neglected (Cappa et al., 2018) and may result, not only from well-known fault arrays but also from preexisting faults that were undetected during the site characterization stage (Husen et al., 2012; Mazzoldi et al., 2012).

Our frictional tests were designed to understand the frictional and transport properties of fault arrays within the OPA formation under conditions relevant to DGR. This study expands upon previous work by exploring saturation conditions, and permeability and dilatancy evolution during shearing. In this way, we have constrained conditions for fault weakness, unstable behavior, and shear dilatancy in the OPA formation. Our results are also consistent with earlier studies about the effects of water on both strength and frictional stability on different clay-rich fault gouges (e.g., Ikari et al., 2007; Morrow et al., 2017; Saffer & Marone, 2003).

Tests on dry gouges show a weak ($\mu_f \approx \mathbf{0.36}$) and unstable behavior at slow sliding velocities that evolves to a stable behavior as soon as a threshold sliding velocity is overcome ($v_* \geq \mathbf{10}$ μm/s). Natural clay-rich faults in the Earth are rarely dry. However, during the operation of the DGR, the heat-generating nuclear waste will significantly change the thermal environment. This will cause near-field drying processes (e.g., temperature and pore pressure gradients) and the surrounding host-rock will tend to dry. Despite this scenario, our results suggest that velocity-weakening behavior in dry clay-rich faults does not persist at high sliding velocities, and therefore, nucleation of large earthquakes is unlikely to occur.

In this study, we have shown that the frictional properties of wet OPA fault gouge are different from the dry counterpart. The wet OPA gouges are weaker ($\mu_f \approx \mathbf{0.16}$) and exhibit a stable, velocity-strengthening behavior at all the σ_n' that are of interest to DGR. This low friction suggests that fault activation may easily occur within the repository; however, fault gouges will slide in an aseismic, stable fashion. Thus, our results may help explain the induced in situ fault reactivation at the MTL; yet they cannot explain the swarm of triggered seismic events (Guglielmi et al., 2017; Jeanne et al., 2018). Because natural faults are complex structures relative to experimental-sized faults, the previously mentioned field observations need to be integrated to additional laboratory work.

Finally, pore volume changes during shearing indicate a dominant shear-enhanced dilation at the onset of fault sliding, in agreement with field-scale experiments at the MT (Guglielmi et al., 2017; Jeanne et al., 2018). However, in our test small permeability increases are within the same range as nondeformed rock values (10^{-20} m^2). These observations suggest that OPA fault arrays can potentially act as poor fluid conduits.

Acknowledgments
Authors are thankful for the financial support of the Swiss Federal Office of Topography (Christophe Nussbaum), the partners of the MTL Project and EPFL. We thank Thierry Adatte for the XRD measurements. We sincerely thank the three anonymous reviewers, Demian Saffer, and the Editor Bayani Cardenas for their suggestions and comments. C.G. thanks the support of the Swiss Federal Office of Energy through the EDGAR project. M.V. thanks the European Research Council Starting Grant project 757290-BEFINE. Data supporting the analysis and conclusions are available in the supporting information.

References

Bar-sinai, Y., Spatschek, R., Brener, E. A., & Bouchbinder, E. (2014). On the velocity-strengthening behavior of dry friction. *Journal of Geophysical Research: Solid Earth*, *119*, 1738–1748. https://doi.org/10.1002/2013JB010586

Baumberger, T., & Berthoud, P. (1999). Physical analysis of the state- and rate-dependent friction law. II. Dynamic friction. *Physical Review B: Condensed Matter and Materials Physics*, *60*(6), 3928–3939. https://doi.org/10.1103/PhysRevB.60.3928

Behnsen, J., & Faulkner, D. R. (2012). The effect of mineralogy and effective normal stress on frictional strength of sheet silicates. *Journal of Structural Geology*, *42*, 49–61. https://doi.org/10.1016/j.jsg.2012.06.015

Bernabé, Y., Mok, U., & Evans, B. (2006). A note on the oscillating flow method for measuring rock permeability. *International Journal of Rock Mechanics and Mining Sciences*, *43*(2), 311–316. https://doi.org/10.1016/j.ijrmms.2005.04.013

Bossart, P., Bernier, F., Birkholzer, J., Bruggeman, C., Connolly, P., Dewonck, S., et al. (2017). Mont Terri rock laboratory, 20 years of research: Introduction, site characteristics and overview of experiments. *Swiss Journal of Geosciences*, *110*, 3–22. https://doi.org/10.1007/s00015-016-0236-1

Brace, W. F., & Byerlee, J. D. (1966). Stick slip as a mechanism for earthquakes. *Science*, *153*(3739), 990–992.

Buscheck, T. A., Rosenberg, N. D., Gansemer, J., & Sun, Y. (2002). Thermohydrologic behavior at an underground nuclear waste repository. *Water Resources Research*, *38*(3), RG3004. https://doi.org/10.1029/2000WR000010

Byerlee, J. D. (1978). Friction of rocks. *Pure and Applied Geophysics PAGEOPH*, *116*(4–5), 615–626. https://doi.org/10.1007/BF00876528

Cappa, F., Guglielmi, Y., Nussbaum, C., & Birkholzer, J. (2018). On the Relationship Between Fault Permeability Increases, Induced Stress Perturbation, and the Growth of Aseismic Slip During Fluid Injection. *Geophysical Research Letters*, *45*, 11,11–12,20. https://doi.org/10.1029/2018GL080233

Crawford, B. R., Faulkner, D. R., & Rutter, E. H. (2008). Strength, porosity, and permeability development during hydrostatic and shear loading of synthetic quartz-clay fault gouge. *Journal of Geophysical Research*, *113*(3), 1, B03207–14. https://doi.org/10.1029/2006JB004634

Cuss, R. J., Milodowski, A., & Harrington, J. F. (2011). Fracture transmissivity as a function of normal and shear stress: First results in Opalinus Clay. *Physics and Chemistry of the Earth*, *36*(17–18), 1960–1971. https://doi.org/10.1016/j.pce.2011.07.080

Dieterich, J. H. (1978). Time-dependent friction and the mechanics of stick-slip. *Pure and Applied Geophysics*, *116*(4–5), 790–806. https://doi.org/10.1007/BF00876539

Fang, Y., Elsworth, D., Wang, C., Ishibashi, T., & Fitts, J. P. (2017). Frictional stability-permeability relationships for fractures in shales. *Journal of Geophysical Research: Solid Earth*, *122*, 1760–1776. https://doi.org/10.1002/2016JB013435

Fang, Y., Elsworth, D., Wang, C., & Jia, Y. (2018). Mineralogical controls on frictional strength, stability, and shear permeability evolution of fractures. *Journal of Geophysical Research: Solid Earth*, *123*, 3549–3563. https://doi.org/10.1029/2017JB015338

Faulkner, D. R., & Rutter, E. H. (2000). Comparisons of water and argon permeability in natural clay-bearing fault gouge under high pressure at 20 °C. *Journal of Geophysical Research*, *105*(B7), 16415–16426. https://doi.org/10.1029/2000JB900134

Faulkner, D. R., Sanchez-Roa, C., Boulton, C., & den Hartog, S. A. M. (2018). Pore fluid pressure development in compacting fault gouge in theory, experiments, and nature. *Journal of Geophysical Research: Solid Earth*, *123*(1), 226–241. https://doi.org/10.1002/2017JB015130

Ferri, F., Di Toro, G., Hirose, T., Han, R., Noda, H., Shimamoto, T., et al. (2011). Low- to high-velocity frictional properties of the clay-rich gouges from the slipping zone of the 1963 Vaiont slide, northern Italy. *Journal of Geophysical Research*, *116*(B9), 1, B09208–17. https://doi.org/10.1029/2011JB008338

French, M. E., Chester, F. M., & Chester, J. S. (2015). Micromechanisms of creep in clay-rich gouge from the Central Deforming Zone of the San Andreas Fault. *Journal of Geophysical Research: Solid Earth*, *120*, 827–849. https://doi.org/10.1002/2014JB011496

Guglielmi, Y., Birkholzer, J., Rutqvist, J., Jeanne, P., & Nussbaum, C. (2017). Can fault leakage occur before or without reactivation? Results from an in situ fault reactivation experiment at Mont Terri. *Energy Procedia*, *114*(November 2016), 3167–3174. https://doi.org/10.1016/j.egypro.2017.03.1445

Heierli, J., & Genoni, O. (2017). The role of temperature in the safety case for high-level radioactive waste disposal: A comparison of design concepts. *Geosciences*, *7*(2), 42. https://doi.org/10.3390/geosciences7020042

Husen, S., Kissling, E., & von Deschwanden, A. (2012). Induced seismicity during the construction of the Gotthard Base Tunnel, Switzerland: Hypocenter locations and source dimensions. *Journal of Seismology*, *16*(2), 195–213. https://doi.org/10.1007/s10950-012-9313-8

Ikari, M. J., Saffer, D., & Marone, C. (2007). Effect of hydration state on the frictional properties of montmorillonite-based fault gouge. *Journal of Geophysical Research*, *112*, B06423. https://doi.org/10.1029/2006JB004748

Ikari, M. J., Saffer, D., & Marone, C. (2009). Frictional and hydrologic properties of clay-rich fault gouge. *Journal of Geophysical Research*, *114*, B05409. https://doi.org/10.1029/2008JB006089

Im, K., Elsworth, D., & Fang, Y. (2018). The influence of preslip sealing on the permeability evolution of fractures and faults. *Geophysical Research Letters*, *45*(1), 166–175. https://doi.org/10.1002/2017GL076216

Jaeger, J., Cook, N. G., & Zimmerman, R. (2007). *Fundamentals of Rock Mechanics*, (4th Edition (4th Editio) ed.). Oxford: Blackwell Publising.

Jeanne, P., Guglielmi, Y., Rutqvist, J., Nussbaum, C., & Birkholzer, J. (2017). Field characterization of elastic properties across a fault zone reactivated by fluid injection. *Journal of Geophysical Research: Solid Earth*, *122*, 6583–6598. https://doi.org/10.1002/2017JB014384

Jeanne, P., Guglielmi, Y., Rutqvist, J., Nussbaum, C., & Birkholzer, J. (2018). Permeability variations associated with fault reactivation in a claystone formation investigated by field experiments and numerical simulations. *Journal of Geophysical Research: Solid Earth*, *123*(2), 1694–1710. https://doi.org/10.1002/2017JB015149

Kohli, A. H., & Zoback, M. D. (2013). Frictional properties of shale reservoir rocks. *Journal of Geophysical Research: Solid Earth*, *118*, 5109–5125. https://doi.org/10.1002/jgrb.50346

Kuwano, O., Ando, R., & Hatano, T. (2013). Crossover from negative to positive shear rate dependence in granular friction. *Geophysical Research Letters*, *40*, 1295–1299. https://doi.org/10.1002/grl.50311

Leeman, J., Saffer, D., Scuderi, M. M., & Marone, C. (2016). Laboratory observations of slow earthquakes and the spectrum of tectonic fault slip modes. *Nature Communications*, *7*, 1–6. https://doi.org/10.1016/0360-3016(81)90183-8

Lefèvre, M., Guglielmi, Y., Henry, P., Dick, P., & Gout, C. (2016). Calcite veins as an indicator of fracture dilatancy and connectivity during strike-slip faulting in Toarcian shale (Tournemire tunnel, southern France). *Journal of Structural Geology*, *83*, 73–84. https://doi.org/10.1016/j.jsg.2016.01.002

Lockner, D. A., Morrow, C., Moore, D. E., & Hickman, S. (2011). Low strength of deep San Andreas Fault gouge from SAFOD core. *Nature*, *472*(7341), 82–86. https://doi.org/10.1038/nature09927

Logan, J. M., & Chester, F. M. (1987). Composite planar fabric of gouge from Punchbowl Fault, California.pdf. *Journal of Structural Geology*, *9*(5/6), 621–634.

Logan, J. M., & Rauenzahn, K. A. (1987). Frictional dependence of gouge mixtures of quartz and montmorillonite on velocity, composition and fabric. *Tectonophysics*, *144*(1–3), 87–108. https://doi.org/10.1016/0040-1951(87)90010-2

Marone, C., & Saffer, D. (2015). The mechanics of frictional healing and slip instability during the seismic cycle. In *Treatise on Geophysics* (Second ed., Vol. 4, pp. 111–138). Elsevier B.V. https://doi.org/10.1016/B978-0-444-53802-4.00092-0

Mazzoldi, A., Rinaldi, A. P., Borgia, A., & Rutqvist, J. (2012). Induced seismicity within geological carbon sequestration projects: Maximum earthquake magnitude and leakage potential from undetected faults. *International Journal of Greenhouse Gas Control*, *10*, 434–442. https://doi.org/10.1016/j.ijggc.2012.07.012

Moore, D. E., & Lockner, D. A. (2004). Crystallographic controls on the frictional behavior of dry and water-saturated sheet structure minerals. *Journal of Geophysical Research*, *109*, B03401. https://doi.org/10.1029/2003JB002582

Moore, D. E., & Lockner, D. A. (2007). Friction of the smectite clay montmorillonite: A review and interpretation of data. In T. Dixon, & C. Moore (Eds.), *The Seismogenic Zone of Subduction Thrust Faults* (pp. 317–345). Columbia University Press. https://doi.org/10.7312/dixo13866-011

Morrow, C., Moore, D. E., & Lockner, D. A. (2000). The effect of mineral bond strength and adsorbed water on fault gouge frictional strength. *Geophysical Research Letters*, *27*(6), 815–818. https://doi.org/10.1029/1999GL008401

Morrow, C., Moore, D. E., & Lockner, D. A. (2017). Frictional strength of wet and dry montmorillonite. *Journal of Geophysical Research: Solid Earth*, *122*, 3392–3409. https://doi.org/10.1002/2016JB013658

Noda, H., & Shimamoto, T. (2009). Constitutive properties of clayey fault gouge from the Hanaore fault zone, southwest Japan. *Journal of Geophysical Research*, *114*, B04409. https://doi.org/10.1029/2008JB005683

Numelin, T. J., Marone, C., & Kirby, E. (2007). Frictional properties of natural fault gouge from a low-angle normal fault, Panamit Valley, California. *Tectonics*, *26*, TC2004. https://doi.org/10.1029/2005TC001916

Nussbaum, C., Bossart, P., Amann, F., & Aubourg, C. (2011). Analysis of tectonic structures and excavation induced fractures in the Opalinus Clay, Mont Terri underground rock laboratory (Switzerland). *Swiss Journal of Geosciences*, *104*, 187–210. https://doi.org/10.1007/s00015-011-0070-4

Orellana, L. F., Scuderi, M. M., Collettini, C., & Violay, M. (2018a). Do scaly clays control seismicity on faulted shale rocks? *Earth and Planetary Science Letters*, *488*, 59–67. https://doi.org/10.1016/j.epsl.2018.01.027

Orellana, L. F., Scuderi, M. M., Collettini, C., & Violay, M. (2018b). Frictional properties of Opalinus Clay: Implications for nuclear waste storage. *Journal of Geophysical Research: Solid Earth*, *123*(1), 157–175. https://doi.org/10.1002/2017JB014931

Ruina, A. (1983). Slip instability and state variable friction laws. *Journal of Geophysical Research*, *88*(B12), 10359–10370. https://doi.org/10.1029/JB088iB12p10359

Rutqvist, J., Cappa, F., Rinaldi, A. P., & Godano, M. (2014). Modeling of induced seismicity and ground vibrations associated with geologic CO_2 storage, and assessing their effects on surface structures and human perception. *International Journal of Greenhouse Gas Control*, *24*, 64–77. https://doi.org/10.1016/j.ijggc.2014.02.017

Rutter, E. H., & Mecklenburgh, J. (2018). Influence of normal and shear stress on the hydraulic transmissivity of thin cracks in a tight quartz sandstone, a granite, and a shale. *Journal of Geophysical Research: Solid Earth*, *123*(2), 1262–1285. https://doi.org/10.1002/2017JB014858

Saffer, D., Frye, K. M., Marone, C., & Mair, K. (2001). Laboratory results indicating complex and potentially unstable frictional behavior of smectite clay. *Geophysical Research Letters*, *28*(12), 2297–2300. https://doi.org/10.1029/2001GL012869

Saffer, D., & Marone, C. (2003). Comparison of smectite- and illite-rich gouge frictional properties: Application to the updip limit of the seismogenic zone along subduction megathrusts. *Earth and Planetary Science Letters*, *215*(1–2), 219–235. https://doi.org/10.1016/S0012-821X(03)00424-2

Samuelson, J., Elsworth, D., & Marone, C. (2009). Shear-induced dilatancy of fluid-saturated faults: Experiment and theory. *Journal of Geophysical Research - Solid Earth*, *114*(12), 1–15. https://doi.org/10.1029/2008JB006273

Scholz, C. H. (2002). *The Mechanics of Earthquakes and Faulting*. New York: Cambridge University Press.

Scuderi, M. M., & Collettini, C. (2018). Fluid Injection and the Mechanics of Frictional Stability of Shale-Bearing Faults. *Journal of Geophysical Research: Solid Earth*, *123*, 8364–8384. https://doi.org/10.1029/2018JB016084

Senger, R., Romero, E., & Marschall, P. (2018). Modeling of gas migration through low-permeability clay rock using information on pressure and deformation from fast air injection tests. *Transport in Porous Media*, *123*(3), 563–579. https://doi.org/10.1007/s11242-017-0962-5

Shimamoto, T., & Logan, J. M. (1981). Effects of simulated clay gouges on the sliding behavior of Tennessee sandstone. *Tectonophysics*, *75*(3–4), 243–255. https://doi.org/10.1016/0040-1951(81)90276-6

Tembe, S., Lockner, D. A., & Wong, T. F. (2010). Effect of clay content and mineralogy on frictional sliding behavior of simulated gouges: Binary and ternary mixtures of quartz, illite, and montmorillonite. *Journal of Geophysical Research - Solid Earth*, *115*(3), 1–22. https://doi.org/10.1029/2009JB006383

Tsang, C. F., Barnichon, J. D., Birkholzer, J., Li, X. L., Liu, H. H., & Sillen, X. (2012). Coupled thermo-hydro-mechanical processes in the near field of a high-level radioactive waste repository in clay formations. *International Journal of Rock Mechanics and Mining Sciences*, *49*, 31–44. https://doi.org/10.1016/j.ijrmms.2011.09.015

Tsang, C. F., Neretnieks, I., & Tsang, Y. (2015). Hydrologic issues associated with nuclear waste repositories. *Water Resources Research*, *51*, 6923–6972. https://doi.org/10.1002/2015WR017641

Wang, W. L., Wang, T. T., Su, J. J., Lin, C. H., Seng, C. R., & Huang, T. H. (2001). Assessment of damage in mountain tunnels due to the Taiwan Chi-Chi earthquake. *Tunneling and Underground Space Technology*, *16*(3), 133–150. https://doi.org/10.1016/S0886-7798(01)00047-5

Wu, W., Reece, J. S., Gensterblum, Y., & Zoback, M. D. (2017). Permeability evolution of slowly slipping faults in shale reservoirs. *Geophysical Research Letters*, *44*, 11,368–11,375. https://doi.org/10.1002/2017GL075506

Yang, S. Y., & Yeh, H. D. (2009). Modeling transient heat transfer in nuclear waste repositories. *Journal of Hazardous Materials*, *169*(1–3), 108–112. https://doi.org/10.1016/j.jhazmat.2009.03.068

Yu, C., Matray, J. M., Gonçalvès, J., Jaeggi, D., Gräsle, W., Wieczorek, K., Vogt, T., et al. (2017). Comparative study of methods to estimate hydraulic parameters in the hydraulically undisturbed Opalinus Clay (Switzerland). *Swiss Journal of Geosciences*, *110*(1), 85–104. https://doi.org/10.1007/s00015-016-0257-9

Zhang, S., & Cox, S. F. (2000). Enhancement of fluid permeability during shear deformation of a synthetic mud. *Journal of Structural Geology*, *22*(10), 1385–1393. https://doi.org/10.1016/S0191-8141(00)00065-1